©2013 IEEE. Accepted May 2013. http://dx.doi.org/10.1109/JSEN.2013.2263496

Pulse Detection by Gated Synchronous Demodulation

Spyros Efthymiou and Krikor B. Ozanyan, *Senior Member, IEEE*

***Abstract*— Synchronous Demodulation (SD) is the signal recovery method of choice when the input envelope signal is modulated by either a pure sine wave or a square wave. SD is less efficient for pulsed periodic signals with a low duty factor. For the latter signals we introduce data processing which applies gating on a part of the signal period to achieve optimum conditions for recovering the pulse amplitude by quadrature SD. The proposed method is evaluated for signal-to-noise performance against Boxcar-type gated integrators in cases of simulated data, as well as data acquired from physical measurements, in the presence of 1/f and Gaussian noise. It is shown that by combining the gating and SD principles, our suggested Gated Synchronous Demodulation outperforms other routine signal processing methods under typical 1/f noise conditions.**

***Index Terms*—gated integration, pulse detection, synchronous demodulation, quadrature detection.**

I. Introduction

THE extensive growth of various types of sensors creates the need to employ new signal detection techniques or modify/customize existing ones. Among factors influencing the layout of the overall detection scheme, the type of the input signal drives the choice of a signal processing technique to achieve, within a certain period of time, a specific Signal-to-Noise ratio (SNR) target at the output. In existing bibliography, the variety of measurement techniques is habitually categorized with respect to the nature of the measured signal [1].

Pulsed excitation is used typically in radiometric applications to study the pulse response of systems, but also to observe physical phenomena where continuous or sinusoidal excitation sources are not available. In the latter case, the priority is to measure one or more parameters linked to the time-averaged energy in the signal, rather than recovering its temporal shape. Instruments that are based on the Synchronous Demodulation (SD) principle are capable of measuring the magnitude and phase of a selected frequency component of the input signal. SD has maximum sensitivity when the input signal is purely sinusoidal or has a duty cycle of 0.5 [1, 2] because the employed modulation-demodulation scheme assumes strictly harmonic functions. In the frequency domain, periodic signals with duty cycle substantially deviating from 0.5 will experience reduction of their magnitude detected at the fundamental frequency because of spreading their energy over higher harmonics. In the time domain, for duty cycle less than 0.5 the signal energy will be smeared over the whole half-period, while for duty cycles larger than 0.5 some signal energy will be lost. In either case of deviation, the pulsed character of the signal becomes essential and the extraction of a single frequency component (usually the fundamental) will no longer be efficient. Under these conditions, gated integration (GI) techniques, such as "boxcar" averagers, are often used to quantify the time-integrated pulsed signal, or completely recover the pulse shape by managing the gate width and timing. Prior to the widespread introduction of digital signal processing (DSP) in measurement systems, measurement trains were often composed of signal recovery tools and instruments connected in series to improve the overall signal detection. An example of such a possible combination is to use GI to extract the pulse amplitude, which is additionally modulated by a carrier wave with period much longer than the pulse rate. The generated output is then offered for quadrature SD[1] (QSD) to extract the low frequency component referenced to the carrier wave. In contrast to SD methods which are now routinely available in digital format [3-5], GI has been embodied mostly in analogue and hybrid implementations [2, 6-11] and rarely in digital [12]. Gated radiometry has been demonstrated in a fully digital system to mitigate the effects of occlusion in particle-rich ambient [13].

In this paper, we present a signal processing method which combines the principle of QSD and GI, to achieve better SNR in pulsed signal measurements. As a first step, the pulse is bracketed by a gating window and the samples outside the window are discarded. The gate duration is calculated to ensure that the periodic signal at the output has an "apparent" duty factor close to 0.5. This signal is then fed continuously for QSD to extract the magnitude and phase of its fundamental component, referenced to a sinusoidal signal with period defined by the gate length. An improved SNR performance results not only from the increase of the average signal energy, but also from the noise reduction inherent to the shift of the baseband to higher frequencies. We introduce this method as Gated Quadrature Synchronous Demodulation (GQSD), to emphasize the synergy between GI and QSD in this case.

Manuscript received August 1, 2012. This work was supported in part by the U.K. Engineering and Physical Sciences Research Council, under Grant EP/E057411/1 "Fast Fibre-Based THz Tomography"

Spyros Efthymiou is with the School of Electrical and Electronic Engineering, The University of Manchester, Manchester, M13 9PL, United Kingdom (e-mail: spyrosefth@googlemail.com).

Krikor B. Ozanyan is with the School of Electrical and Electronic Engineering, The University of Manchester, Manchester, M13 9PL, United .Kingdom (tel. +44 161 306 4787; e-mail: k.ozanyan@manchester.ac.uk).

[1] The technique is commonly referred to as quadrature synchronous detection, lock-in amplification or phase sensitive detection. In this paper the acronym QSD as also pertains to an instrument implementing the method: "Quadrature Synchronous Detector

To compare the GQSD performance to SD and GI requires the use of comparable DSP tools within the same processor unit to ensure identical bandwidth and processing power. Therefore, to allow a valid comparison, all three methods were separately implemented and tested in NI LabVIEW.

As a summary of existing literature, Section II formulates the principles of operation of digital SD and GI in the discrete time domain. GQSD is introduced in detail with flowcharts and mathematical expressions in Section III. Section IV includes the GQSD performance evaluation by numerous simulations and experiments, the results of which are analyzed in Section V. The end of the paper summarizes the work and mentions briefly an example where GQSD may offer an advantage with low bandwidth receivers such as pyroelectric detectors (PED) [14].

II. BACKGROUND

A. Quadrature Synchronous Detection

The energy content of a pulse train is defined by the product of the maximum peak power P_{pk} and pulse width χ for regular pulse shapes. The energy of pulse trains is often characterized by the average power P_{avg} equal to the product of P_{pk} and duty cycle δ as shown in (1) where δ is the ratio between the pulse width χ and the pulse repetition time T_0.

$$P_{avg} = \frac{\chi}{T_0} P_{pk} = \delta P_{pk} \tag{1}$$

In a wide range of applications, it is often required to measure the pulsed transmitted energy, either by means of average power or the pulse peak amplitude when the pulse shape is known. Commonly, methods such as shifting the baseband to higher frequency with subsequent QSD are used to achieve SNR improvement with respect to the input noise conditions.

Experiments exploiting QSD use a periodic reference signal $r[k]$ that is usually derived from the modulation source. The detected input signal $s[k]$ is multiplied with $r[k]$ in order to establish the correlation between the two. This is shown in (2) where $s_c[k]$ is the noise-free signal of interest, $n[k]$ represents any accompanying noise and interference and k enumerates the discrete samples:

$$y[k] = r[k]s[k] = r[k]\{s_c[k] + n[k]\} \tag{2}$$

When both, the signal $s_c[k]$ and the reference $r[k]$ are samples of strictly harmonic functions of the same frequency f_r, the product $r[k]s_c[k]$ will give rise to a higher frequency harmonic $2f_r$ along with a DC component proportional to their phase difference $\Delta\theta$. Consequently, the higher frequency component at the system's output can be suppressed by a low pass filter (LPF), leaving only the demodulated baseband as the low frequency envelope containing the variation of the pulse amplitudes with time. On the other hand, a normally distributed noise is completely uncorrelated with the reference signal therefore, the product will randomly fluctuate between positive and negative values exhibiting a normal distribution [15] around the zero. The width of the distribution reflects on the bandwidth where the cut-off frequency, as well as the order, of the LPF is the essential margin of the noise contribution to the output signal.

QSD is achieved by multiplying the input signal $s[k]$ with a pair of reference quadrature sinusoids ($i[k] \equiv r[k]$ and $q[k]$ which is $\pi/2$ phase-shifted from $r[k]$) as shown in (3):

$$\begin{aligned} y_i[k] &= s[k]i[k] \\ y_q[k] &= s[k]q[k] \end{aligned} \tag{3}$$
$$i[k] = \sin(2\pi f_r kT_s); q[k] = \sin(2\pi f_r kT_s + \pi/2)$$

where T_s is the sampling period. Each of the two products in (3) is low pass filtered to obtain the "in-phase" and "quadrature" baseband components, $I[k]$ and $Q[k]$ respectively.The vector magnitude $R[k]$ and phase $\varphi[k]$ of the frequency component of $s[k]$ correlating with $r[k]$ are:

$$R[k] = \sqrt{I^2[k] + Q^2[k]} \tag{4}$$

$$\phi = \tan^{-1}\left\{\frac{Q[k]}{I[k]}\right\} = \Delta\theta[k] \tag{5}$$

where $\Delta\theta$ is the phase difference between the harmonic of interest and reference signal. The main noise reduction achieved by the QSD is due to the LPF with a cut-off frequency (f_{-3dB}), yielding output bandwidth B_{out}. The output bandwidth of a single pole LPF is estimated by (6):

$$B_{out} = f_{-3dB} = \frac{1}{2\pi\tau_{sd}} \tag{6}$$

where τ_{sd} denotes the time constant of the filter. A general expression of the Signal-to-Noise Improvement Ratio (SNIR) is given by [15]

$$SNIR = \sqrt{\left(\frac{B_{in}}{B_{out}}\right)} \tag{7}$$

where B_{in} is the input bandwidth. The expression in (7) is considered valid in the cases with white noise and unity gain [1, 15] filter response. Since B_{out} is essentially the bandwidth of the output LPF, SNIR increases as f-3dB is decreased. An attractive feature of modulation followed by QSD is the ability to reject low frequency drifts and noise signals with power spectral densities proportional to $1/f^{\beta}$ ($0 < \beta < 3$). This principle is based on the idea of shifting (modulating) a low frequency component, to a higher frequency where 1/f noise falls below the white noise floor. Without modulation (no chopping), the spectrum of the detected signal would consist of the baseband containing noise and interference inherited from integrated electronics, external vibrations, interfering electromagnetic fields etc. Figure 1 illustrates the Fourier spectrum of pink noise and two sinusoidally modulated signals; signal A at 2 Hz and signal B at 1 kHz. Assuming equal magnitudes of the two

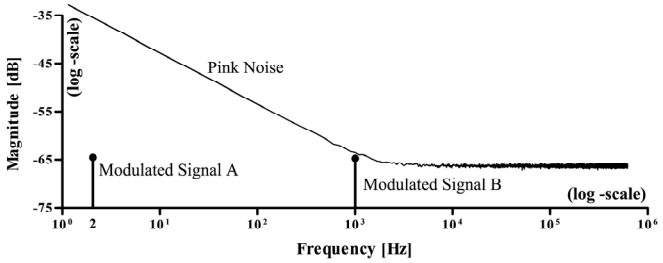

Fig. 1 Exemplified frequency spectrum of a detected modulated signal signifying the importance of modulating signals at higher frequencies

signals, demodulation at 1 kHz results in SNR advantage of approximately 30 dB.

B. Gated Integration

GI is achieved by integrating the input signal during a predefined time aperture, or gating window (GW), opening after a controlled delay relative to an applied trigger. A static mode gated integrator (SMGI) uses a fixed delay and is therefore continuously integrating a fixed time segment within the period of the input signal. A recovery mode GI (RMGI) applies a variable delay on a narrow GW, thus scanning it across the input signal. This results in the recovery of the temporal shape of the input signal in non-real time.

The typical analogue implementation of GI is based on a controllable switch connected in series with an integrating RC circuit. The start and duration of the GW are defined by a binary gating signal $g(t)$. Integration of the input signal $s(t)$ occurs only when $g(t)$ is high (gate open). A negative edge of $g(t)$ disconnects the input signal from the integrator and the latter is connected to an RC network capacitor for storage.

If the voltage droop due to charge leakage is eliminated, after a sufficient number of gates the storage capacitor is charged to a voltage approximating the average value of the gated segment of the input signal. Depending on the nature of the averaging (exponential or linear) the output rises asymptotically towards the average value in the gated segment or increases by adding every consecutive sample, yielding the average by division to the number of gates.

The SNR improvement achieved by linear gated averaging is equal to the square root of the number of consecutive gated samples [1, 8]. In addition to linear averaging, commercial GI units[2] incorporate exponential averagers with performance similar to a simple RC LPF. The SNIR achieved in exponential averaging is given by

$$SNIR_{EA} = \sqrt{\frac{2\tau_{GI}}{M}} \tag{8}$$

where τ_{GI} and M are the integrator time constant and duration of the GW respectively. Exponential averaging is described by a simple relationship between the input and output signal levels and therefore the targeted SNIR can be obtained by appropriately selecting the values of τ_{GI} and M.

Although linear averaging gives better SNIR at a large number of repetitions, the difference between the two becomes negligible if the exponential averaging time is at least five time constants ($5\tau_{GI}$). It is important to note here that the observed bandwidth determined by the integration-storage sequence depends on the time constant of the storage RC network, as well as the gate size and repetition period. Further, we take as an example an exponential SMGI employing a first order LPF defining the bandwidth by its frequency response. Similar to a QSD, the cut-off frequency of the LPF is similar to (6) but with time constant τ_{GI}. The ratio between the time constant τ_{GI} and the gate length M defines the amount of pulse periods needed until the output of the LPF reaches 63% of its steady-state response. When this value is multiplied by the period of the input pulse train it yields to the observe time constant (OTC) of the GI given by (9).

$$OTC = \frac{\tau_{GI}}{M} \times \frac{T_0}{T_s} \text{ for } \tau_{GI} > T_s \cdot M \tag{9}$$

When τ_{GI} is less or equal than M, the OTC is defined by the effective time constant (ETC) of the LPF (τ_{GI}). The bandwidth of a SMGI is defined by the cut-off frequency of the LPF regardless to the OTC. The bandwidth of a RMGI is out of the scope, nonetheless detail analysis can be found in [1].

C. Noise performance and SNIR

GI may be considered as repetitive averaging and is often used to minimize the effect of broadband (white) noise [16] by bandwidth narrowing. It also maximizes the detected signal amplitude. However, in the presence of flicker noise the SNR performance of a SMGI is unsatisfactory; this becomes obvious when it is analyzed in the frequency domain. Gated integration is equivalent to filtering of a continuous signal assembled from consecutive signal blocks which are made adjacent by the gating signal $g(t)$, since signal integration takes place only when the gate is open. For GWs of any size, a SMGI operates at the baseband region of the spectrum extracting a low-frequency envelope. Even with sharp and narrow bandwidth LPFs, the most substantial part of Flicker noise will still appear at the output, significantly degrading the SNIR.

QSD, on the other hand, selects (and possibly amplifies) baseband frequency components after they are shifted to a part of the spectrum where the effect of flicker noise is significantly reduced. However, QSD is sensitive to the duty factor deviating from 0.5 as this suppresses the magnitude of the detected signal.

The complementary merits of QSD and SMGI are often conspicuous in literature, but are usually limited to the case where only the type and shape of the input signal is considered [1], as opposed to detecting an average value. Further, we introduce the new method of GQSD and compare it to the noise performance of SMGI. For that we have developed a LabVIEW based simulator [17] allowing detailed and extensive analysis of the two methods, involving different types of noise sources.

III. Gated Quadrature Synchronous Detection

A. Introduction

It has already been mentioned that the sensitivity and efficiency of QSD is greatly reduced when low duty cycle pulse trains are considered. In this section we analyze that in more detail and introduce the algorithm for implementing GQSD which is suitable for pulsed signals of low duty cycle. This algorithm is based on the principles of GI and SD and minimizing the effect of Flicker noise, while enhancing the signal, thus improving the output SNR. The utilization of baseband shifting and QSD ensures minimum contributions

[2] C.f. EG&G 162 mainframe boxcar averager, where gated integration is performed in separate processor modules (163 and/or 164)

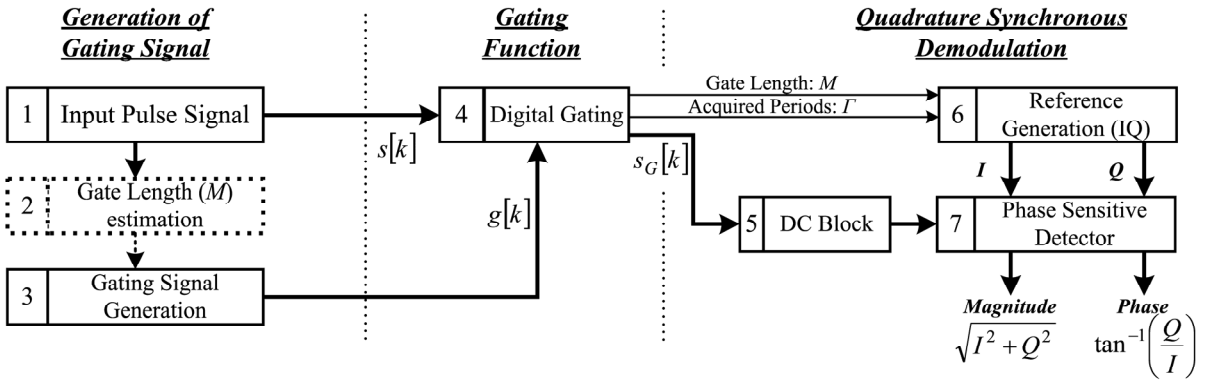

Fig. 2 Block diagram of a digital GQSD with 3 sections: Gating Signal generation, Gating Function and QSD.

from flicker noise while the gating function conditions the signal for the application of synchronous detection.

B. Theory of Operation

The structure of GQSD is broken down in three sections as illustrated in Fig. 2. The signal processing throughout each section of GQSD is illustrated in Fig. 3, where for each section the resulting discrete time domain signals are presented on the left hand side of the figure. The right hand side of the figure describes the process in the Fourier domain showing the effect of gating.

1) Generation of the Gating Signal

As shown in Fig. 2, the first block is responsible for the acquisition (from measurements or simulation) of the pulsed input signal $s[k]$. The remaining two blocks are used to generate the gating signal $g[k]$. Therefore, to introduce this block properly, it is necessary to involve also the effect of $g[k]$ on the output of the next section (Gating Function), which is the gated signal $s_G[k]$.

The opening of the gate (low to high transition of $g[k]$) and its duration ($g[k]$ high) are given in units of k by D and M respectively (see Fig. 3). Since the output from the gating stage $s_G[k]$ is formed by a continuous concatenation of the gated segments taken from the input signal, the purpose of block 2 in Fig. 2 is to estimate the value of M which maximizes the magnitude of the fundamental frequency in $s_G[k]$. This is accomplished by computing the discrete time Fourier series (DTFS) of the pulse input train. Following [18] the general expression of discrete Fourier series representation of a function $f[k]$ is:

$$f[k]=\sum_{h=0}^{N_0-1}\Im_h e^{jh\frac{2\pi}{N_0}k} \tag{10}$$

$$\Im_h=\frac{1}{N_0}\sum_{k=0}^{N_0-1}f[k]e^{-jh\frac{2\pi}{N_0}k} \tag{11}$$

where k and h enumerate respectively the samples and harmonics of $f[k]$; $\Im_h$ and N_0 denote respectively the magnitude of h-th constituent harmonic and the period (in units of k) of $f[k]$. Therefore the DTFS of the pulsed input train $s[k]$ is given by [18]:

$$s[k]=\frac{AX}{N_0}+\frac{A}{N_0}\sum_{h=0}^{N_0-1}\frac{\sin\left(X\frac{\pi}{N_0}h\right)}{\sin\left(\frac{\pi}{N_0}h\right)}\cdot e^{jh\frac{2\pi}{N_0}k} \tag{12}$$

where A is the pulse amplitude and X is the pulse width (in units of k). The second term gives the magnitude sum of the harmonics that are contained within the input signal.

The h=1 term in (12) represents the magnitude $\Im_1$ of the fundamental harmonic of $s[k]$:

$$\Im_1(N_0)=\frac{A}{N_0}\frac{\sin(X\pi/N_0)}{\sin(\pi/N_0)} \tag{13}$$

The function $\Im_1(N_0)$ in (13) has a maximum at $N_0^{\max}=M=2X$, which corresponds to a duty cycle $\delta=0.5$.

2) Gating Function

A single period of the gating signal $g[k]$ consists of L

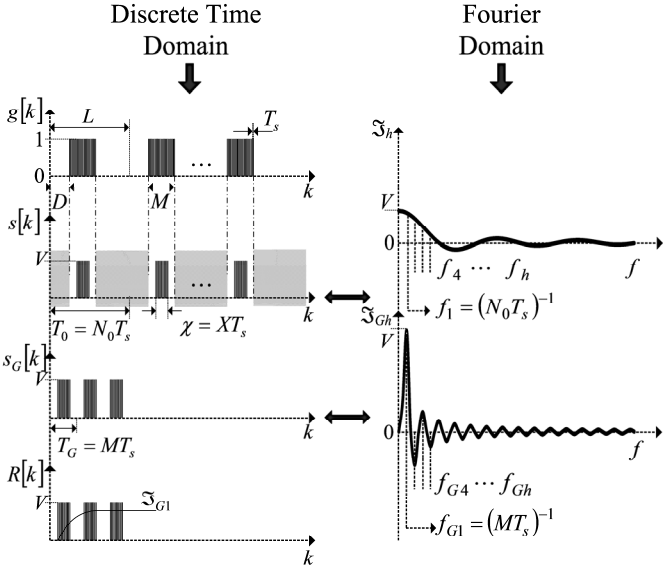

Fig. 3 Illustration of the resulting discrete time domain signals of each section of GQSD along with the Fourier spectrum. The notation used in the figure is also used throughout the text and equations of this paper.

samples. By setting $L=N_0$, each sample of the input signal $s[k]$ can be selected or discarded according to the value of the

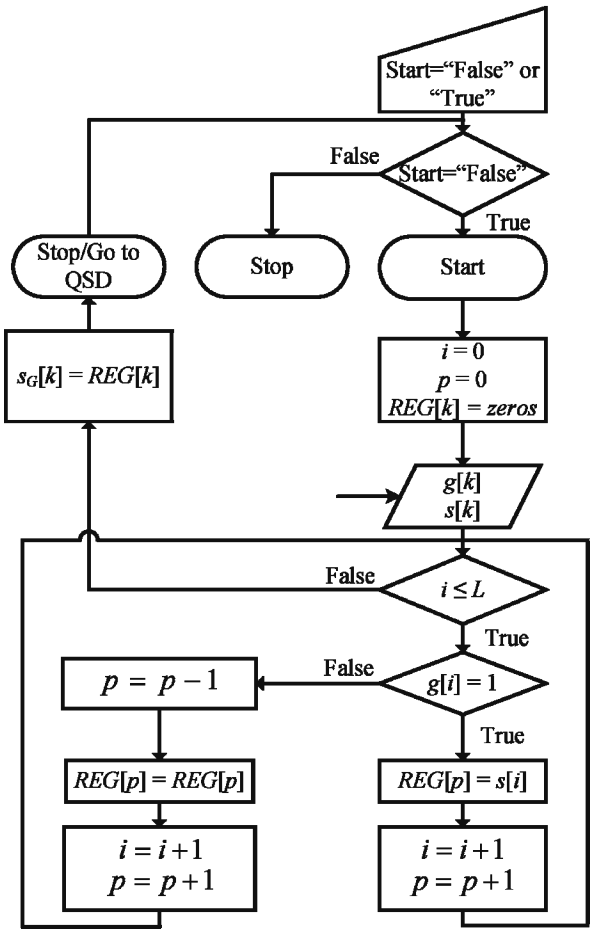

Fig. 4 Flowchart of the gating function algorithm.

corresponding element of $g[k]$. The algorithm for the digital gating (block 4) in Fig. 2 is described by the flowchart in Fig. 4. The open gate is represented by unity values of $g[k]$ while the closed gate is represented by zeros. Since $L = N_0$, the signal index k and gating index i are identical and the loop runs only on a single index i.

Under an open gate condition ($g[i]$=1), the i^{th} element of the input signal $s[i]$ is stored in a register *REG* at a position specified by a separate index p. Thus, the loop index i enumerates the input signal samples, while p enumerates the samples in the resulting gated output signal $s_G[k]$. When the loop index i runs through the complete period of $g[k]$, the content of the register is passed to the QSD and the process is repeated. Consequently, *REG* contains the new discrete signal $s_G[k]$ for the current period only and concatenates adjacent periods by discarding the incoming samples when the gate is closed. Consider now that the gate length is optimized in section 1 (see Fig.2) and N_0 is replaced by M. Then the DTFS of $s_G[k]$ is expressed by:

$$s_G[k] = \frac{AX}{M} + \frac{A}{M}\sum_{h=1}^{M-1} \frac{\sin\left(X\frac{\pi}{M}h\right)}{\sin\left(\frac{\pi}{M}h\right)} \cdot e^{jr\frac{2\pi}{M}k} \qquad (14)$$

The $h = 1$ term again represents the magnitude $\Im_{G1}$ of the fundamental harmonic of $s_G[k]$ and δ_G defines the duty cycle of the modified signal $s_G[k]$:

$$\Im_{G1}^{\max} = \frac{A}{M}\frac{\sin(\delta_G \pi)}{\sin(\pi / M)}; \quad \delta_G = \frac{X}{M} = 0.5 \qquad (15)$$

3) Quadrature Synchronous Detection

QSD takes place within blocks 6 and 7 of section 3 in Fig.2. The principle of operation of a QSD is discussed in section II of the paper and here we focus on aspects relevant only to the gated character of $s_G[k]$ and GQSD in general. Block 6 generates the reference signals $i[k]$ and $q[k]$. The product of each of these references reference with $s_G[k]$ yields the real ($I[k]$) and imaginary ($Q[k]$) components of the referenced harmonic. The period length of the reference signals (in units of k) is set equal to M and the optimal gate length is determined in block 2 (see Fig. 2).

Referencing towards M ensures selective demodulation from a discrete carrier wave specified by the optimized gating period, as opposed to the pulse repetition rate. IIR LPFs are used to extract the DC term of $I[k]$ and imaginary $Q[k]$ and subsequently compute the magnitude of the demodulated complex vector according to [4].

To validate and compare the GQSD with an SMGI, infinite impulse response (IIR) filters are used in all methods to mimic classical analogue LPF structures. The algorithm employs two 1st order Butterworth filters with a cut-off frequency defined by (6). In addition to the LPFs of the PSD, a 1st order Butterworth high pass filter (HPF) is utilized in block 5 of Fig. 2, to attenuate the DC component of $s_G[k]$, diminishing its contribution to the output signal. Similarly to a SMGI, the time response of GQSD is affected by the gate length resulting to an observed time constant (OTC) as described by (16) where τ_{sd},T_0, and T_s are the time constant of the LPF, the pulse period, and the sampling time, respectively (in sec), whereas M specifies the gate width (in number of samples).

$$OTC = \frac{\tau_{sd}}{M} \times \frac{T_0}{T_s} \text{ for } \tau_{sd} > MT_s \qquad (16)$$

4) Determining M for an arbitrary pulse shape

The fundamental component $\Im_{G1}$ reaches maximum when δ_G becomes 0.5, therefore $M = 2X$ can be calculated from X. However, X is easy to quantify only in the trivial case of a train composed of perfectly rectangular pulses. In practice, (e.g. radiation measurements) the pulse shape will depend on the characteristics of the emitter and receiver. When the pulse shape is complex but reproducible, $\Im_{G1}$ can be estimated by comparing its value with M as parameter. The solid line in Fig. 5a represents a rectangular pulse pattern, repeating every 250 samples (i.e. N_0=250). In this example the width of the emitter pulse contains 25 discrete samples resulting in a duty cycle of 0.1. The dashed line plot illustrated in Fig. 5a shows the receiver's steady-state response (simulated in COMSOL Multiphysics for a pyroelectric detector (PED) SPD-42[18]). Figure 5b shows how M is determined numerically by finding the maximum from multiple FFT calculations of $\Im_{G1}$ for a gate size that varies in unit increments from 1 to N_0.

Noticeable in Fig. 5b is the difference between the two plots corresponding to the rectangular excitation pulse (bold) and the PED response (dashed). In the former case, concatenation with new samples of the same value (up to k=25) does not contribute to a harmonic function and $\Im_{G1}$ is zero. The latter plot manifests a double peak – the first maximum is caused by the PED response peaking half way through the excitation pulse while the second corresponds to a harmonic contribution (k=45) resulting from the positive to negative swing. The position of the second maximum is determined by the value of k for which the area under the signal becomes zero, resembling δ_G of 0.5.

IV. Evaluation Setup

Here we aim to evaluate the performance of GQSD on data trains which are either simulated or acquired experimentally from a radiation measurement. The development of the GQSD method has resulted in embedding it in a fully interactive, LabVIEW-based signal processing simulator (SPS), originally developed as a PED simulator [18], for transient and frequency response analysis of a PED model [17]. All evaluations in this work were performed within the SPS environment: the digitally simulated or physically acquired signals are presented in an identical manner to the input of GQSD and alternative methods implemented in SPS, regardless of the mode of operation (simulation or acquisition).

As mentioned earlier, the output signal level of a conventional QSD (CQSD) suffers a significant drop as the duty cycle of the input pulse train decreases, consequently deteriorating the output SNR.

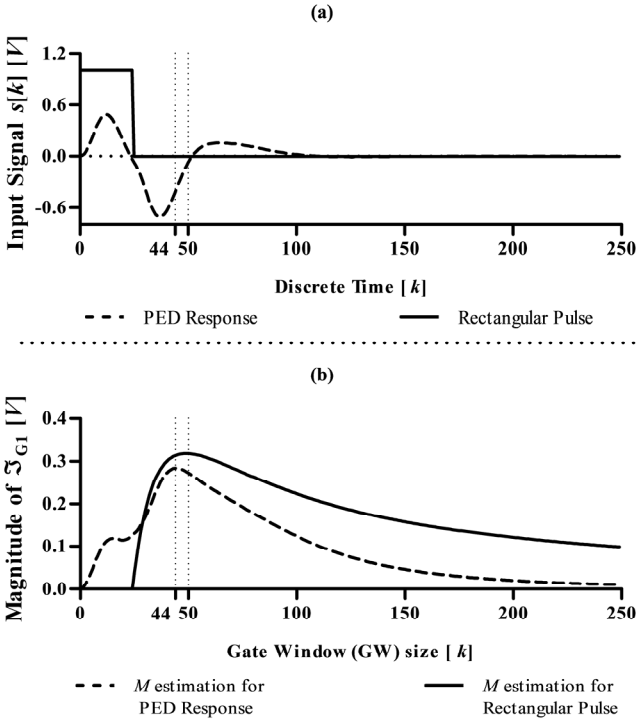

Fig. 5 Estimation of the optimal value of M. A rectangular pulse pattern (solid line) and a typical steady-state response of a PED (dashed line) are shown in (a). For each input, the maximum value of $\Im_{G1}$ signifies the optimal value of M (b).

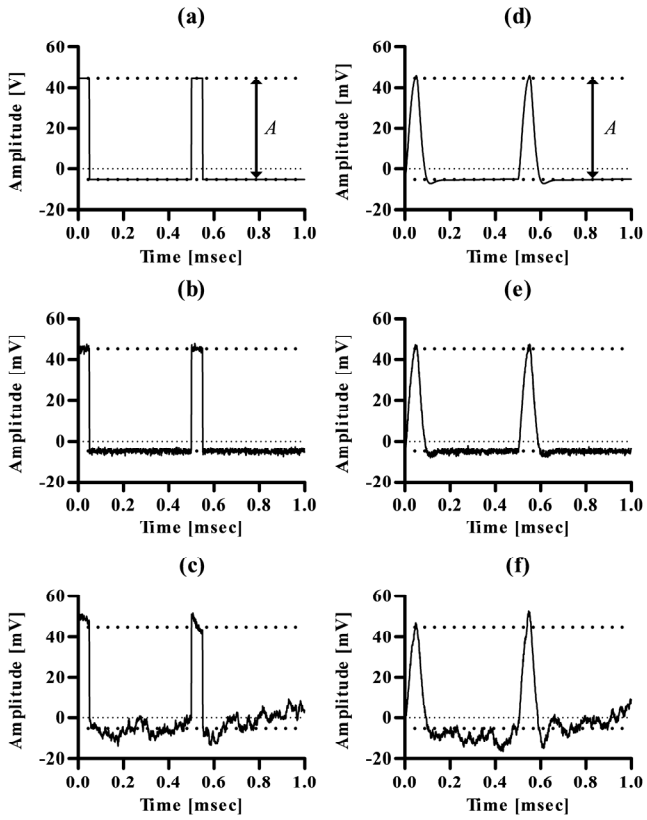

Fig. 6 Simulated pulsed signals of ideal (on the left) and realistic (on the right) shape. a) and d) – noise free; b) and e) – with Gaussian noise; c) and f) – with flicker noise.

Contrary to this, the gating function of GQSD prevents the output signal from dropping at low duty cycles and the SNR output remains at high levels. This obvious SNR improvement in GSQD against CQSD has been confirmed by processing of pulsed trains; for duty cycle of 10% GQSD outperforms with around 5dB and with much more at lower values of the duty cycle. Therefore, further we focus on evaluating GQSD against SMGI only, using SNR as the main criterion. The results obtained from either method are compared and summarized in section V.

A. Simulated Data

The simulation setup refers to a pre-specified set of input signal parameters, noise levels, and settings with respect to the type and objectives of the simulation.

1) Cases for Evaluation

A number of cases are considered depending on the type of the input pulsed signal. The first one (Case A) investigates performance when detecting rectangular pulse trains while the second (Case B) deploys the two methods in a realistic environment, with realistically shaped pulsed signals generated by SPS. In both cases the input signals are accompanied with Gaussian white and/or colored noise, synthesized by fully adjustable noise generators.

TABLE II
GATE SIZE AND BANDWIDTH SETTINGS

M [samples per gate]	f_{eff} [Hz]	*ETC* [ms]	*OTC* [ms]
4	50.000	3.18000	497.36
4	775.01	0.20536	32.087
4	1700.0	0.09362	14.628
62	3.2260	49.3380	497.36
62	50.000	3.18000	32.087
62	109.679	1.45110	14.628
136	1.4700	108.230	497.36
136	22.790	6.98210	32.087
136	50.000	3.18000	14.628

The effect of various types of colored noise on the output SNR of GQSD and SMGI is examined in Case C. The time domain representation and parameters of the signals used in case A, B and C, are shown in Fig. 6 and Table I.

To allow comparison between performance between acquired and simulated data, a forth case (Case D) simulates the voltage response of a PIN photodiode exposed to a pulsed modulated radiation. The input signal in Case D, matches the experimentally acquired one, described in IV.B, along with the experimental setup.

2) Input Signal

Rectangular pulsed trains (Case A) are produced by standard function generators available within the LabVIEW libraries. The generation of arbitrary pulsed signals (Case B), is achieved by feeding the rectangular pulse train to the input of a Transfer Function (TF) within the SPS. Therefore the shape of the resulting time domain signal depends on the characteristic polynomial of the TF. This allows the simulation of the sensors provided that their TF is realizable. [17,19]. Under ideal input conditions (noiseless input), the output of the GQSD and SMGI methods represents the "true" output which is subsequently used to estimate the relative error when noise is taken into account.

The synthesized ideal and non-ideal signals are shown in Fig. 6a and Fig. 6d. Further, Fig. 6b and Fig. 6e illustrate the two signals with additional Gaussian noise. Lastly, Fig. 6c and Fig. 6f depict that same signal immersed in 1/*f* noise. Noise is synthesized by corresponding LabVIEW subroutine algorithms and then is added to the input to construct noisy signals. Gaussian white noise generation is achieved by converting uniformly distributed random numbers into a Gaussian distributed sequence. Unlike to the flat spectrum of white noise, the power spectral density *P*(*f*) of colored noise is inversely proportional to the frequency [20] as shown in (18):

$$S(f) \propto \frac{1}{f^{(\beta)}} \tag{17}$$

The color of the noise is defined by the exponent β ($0 < \beta < 3$), including white ($\beta = 0$), pink ($\beta = 1$) and brown ($\beta = 2$). The noise generating algorithm permits the synthesis of any noise color specified within the range of β by feeding white noise though a dynamic system, usually a shaping filter. While Case A and Case B involve white and pink noise respectively, Case C introduces the variety of noise signals, as shown in Fig. 7 a,b,c, where β takes values between $1.5 < \beta < 2.5$. Within this range we aim to demonstrate the SNR improvement in the case of GQSD as the noise colour shifts from pink to brown (β = 1.5), brown ($\beta = 2$) and beyond ($\beta = 2.5$). The log-log power spectra of Fig. 7a, Fig.7b and Fig. 7c exhibit the three values of slope β, as estimated by (18), with Δy denoting the magnitude difference in dB and Δx corresponding to a frequency range of 1 octave.

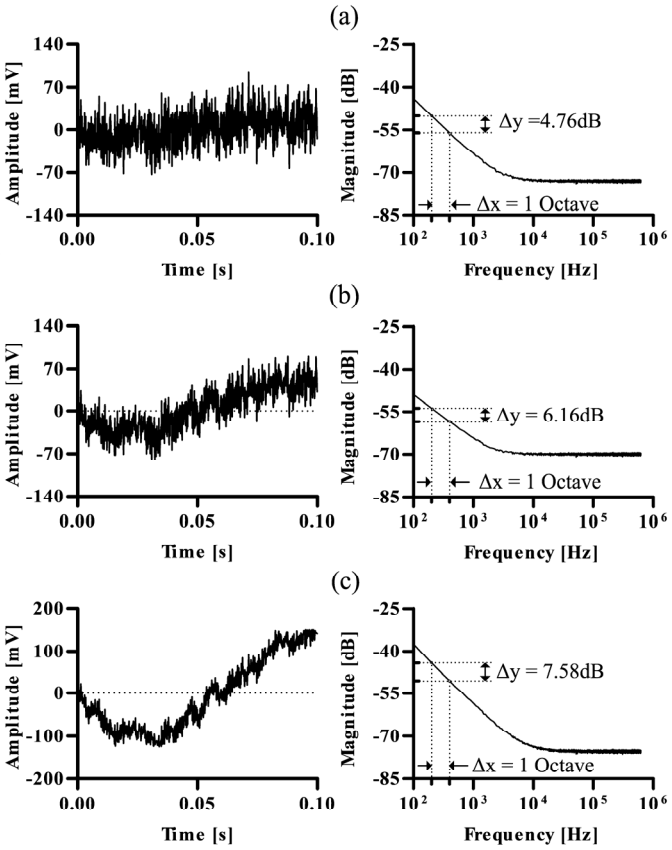

Fig. 7 Time (left) and frequency (right) domain representation of simulated colored noise. The PSD in (a) is proportional to $1/f^{\beta}$ for $\beta = 1.58$, (b) $\beta = 2.04$ and (c) $\beta = 2.23$

TABLE I
INPUT SIGNAL PARAMETERS VALUES

Symbol	Description	Value	Units
A	Pulse Peak Voltage	50	*mV*
f_0	Pulse modulation frequency	2	*kHz*
T_0	Pulse modulation period	0.5	*ms*
δ	Duty cycle	≈10	*%.*
N_0*	Samples per period	625	*samples*
X*	Samples per pulse	63	*samples*

* The discrete period of the signal is estimated from the product $T_0 \cdot f_s$, where "f_s" denotes the sampling rate. The number of samples per pulse is estimated by $N_0 \cdot \delta$.

$$\beta = \frac{\Delta y}{10\log(f_2) - 10\log(f_1)} = \frac{\Delta y}{10\log(\Delta x)} \tag{18}$$

3) Sampling and Processing Settings

The generation or acquisition of the discrete input signals is achieved under a pre-specified sampling rate (f_s) and time frame (t_{sim}) defined by the amount of processed pulsed periods.

Assuming a hypothetical sampling rate of 250 kHz, the overall discrete size of a 60 sec input signal becomes very large (15MSamples). To avoid degradation of computational performance, the simulation/acquisition of the input signal is broken into smaller segments utilizing single feedback nodes to pass the final values as initial conditions for the next simulation/acquisition segment. This enables continuous data processing without excessive strain on computer memory (RAM).

The main goal of the evaluation procedure is to determine the SNIR of each method under various types of pulsed signals and noise. According to (9) and (16), the OTC of SMGI and GQSD is proportional to the effective bandwidth (f_{eff}) of their internal LPFs and the size of the gate M. Useful comparison between the two methods is possible only if their OTCs are equal. With respect to the gate size M, the f_{eff} must be adjusted so that the OTC reaches the desired value. Table II shows the calculated correspondence between gate size and bandwidth settings for three values of the sampling rate measured in units of samples per gate duration. In the example on the bottom row, assume that the GQSD of 50Hz effective bandwidth utilizes a gating signal of 136 samples gate width (M) to detect a rectangular pulsed train: this setting yields an OTC of 14.628ms.

In an example comparison with the performance of SMGI for M = 4 samples, the f_{eff} must increase to 1.7kHz to meet the required OTC of 14.628ms. Alternatively, decreasing the f_{eff} to 1.47of GQSD while the f_{eff} of SMGI remains at 50Hz the two methods can be compared at a higher OTC (≈ 497ms). Following this approach we compute the output SNR of GQSD and SMGI for various values of M at a specified f_{eff}. For each gate length the SNR is computed for all possible values of OTC by adjusting the f_{eff} accordingly.

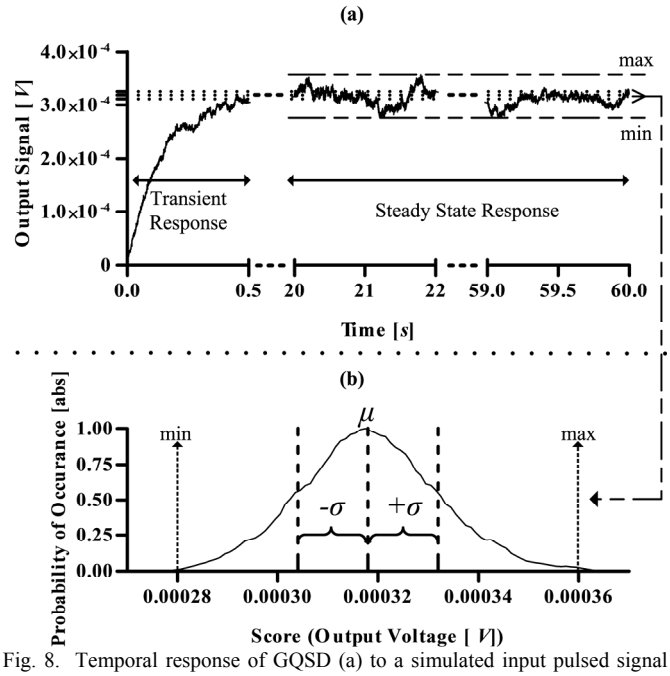

Fig. 8. Temporal response of GQSD (a) to a simulated input pulsed signal immersed in flicker noise. The probability density distribution of its steady state response is shown in the bottom (b), where *min* and *max* correspond to -3σ and +3σ, respectively

4) Estimation of the output SNR and Relative Error

The computation of the output SNR requires the analysis of signals obtained at the output of the method under test (MUT). Under noisy conditions, statistical analysis is imperative to ensure the fidelity of the output average to the quantity being measured. Consider the case of a continuous measurement on a time-domain output signal shown in Fig. 8. The estimated output SNR (SNR_{est}) is defined by the ratio of the mean (μ_{est}) to the standard deviation (σ) of the output measured signal (19). To find the true (expected) SNR value it is necessary first to run the simulation without noise and record the mean (μ_{exp}) of the response. Subsequently the ratio between μ_{exp} and the estimated standard deviation of the noise (σ) yields the expected SNR (SNR_{exp}) as shown in (20) while the relative error (E_r) is estimated by (21)

$$SNR_{est} = \frac{\mu_{est}}{\sigma} \tag{19}$$

$$SNR_{exp} = \frac{\mu_{exp}}{\sigma} \tag{20}$$

$$E_r = \frac{\mu_{est} - \mu_{exp}}{\mu_{exp}} \tag{21}$$

B. Experiments

For this task, SPS operates in acquisition mode and uses NI acquisition hardware (NI USB-6251), permitting up to 1.25MHz sampling rate. The block diagram of the hardware setup is shown in Fig. 9. The digital function generator (DFG) TTi 1010 is used to drive a basic red laser diode with a rectangular pulsed signal of 2 kHz frequency and duty cycle of 0.0048. Detection of the emitted radiation was achieved by a PIN photodiode transducer (PDA10CS) operating in trans-impedance mode.

The signal is amplified by a generic non-inverting amplifier and subsequently digitized by the NI USB-6251 at the specified sampling rate. To ensure synchronous detection and avoid custom made triggering circuits, a reference signal (TTL level) originating from the DFG was connected to the digital ports of the NI USB-6251 to trigger the acquisition.

The detected signal is processed by the two methods to measure the output signal and noise levels. Subsequently, these values are used to compute their SNR performance. The results obtained in Case D of the simulations are compared with the experimental findings.

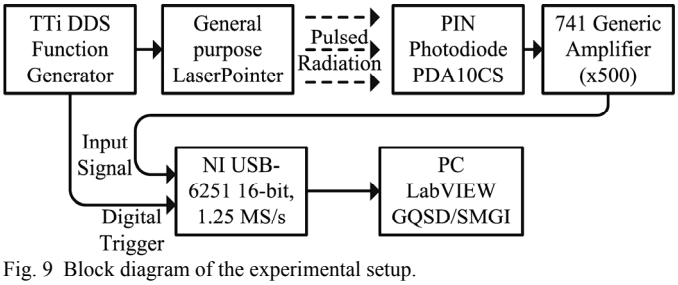

Fig. 9 Block diagram of the experimental setup.

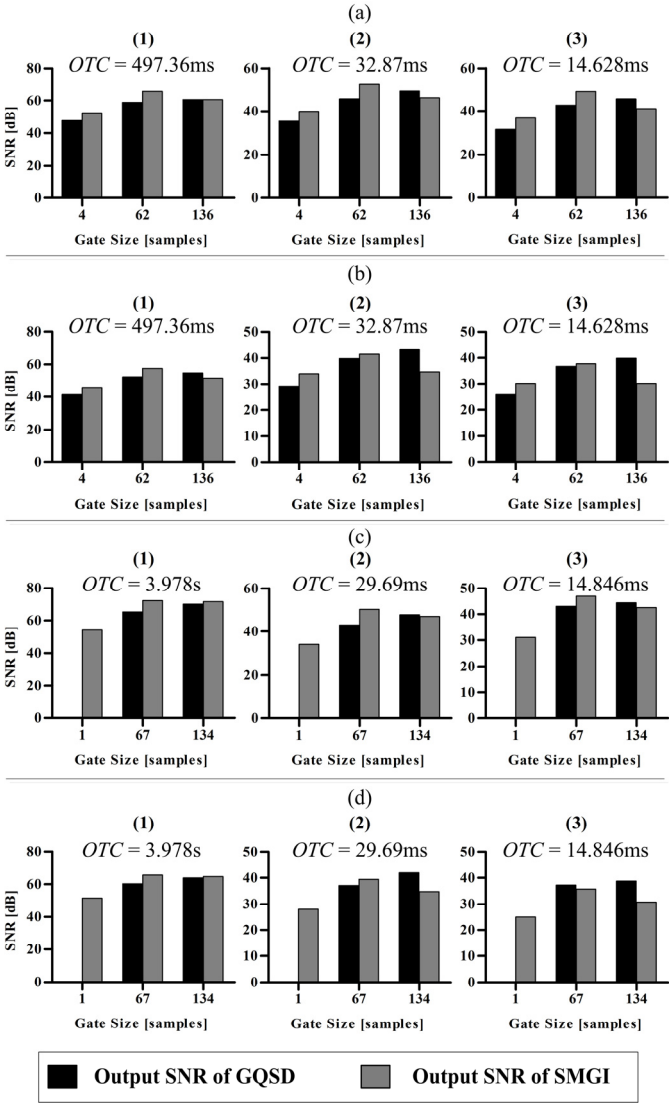

Fig. 10. Simulated SNR performance of GQSD (black bars) and SMGI (grey bars). The charts in (a) and (b) correspond to Case A, and the bar charts in (c) and (d) to Case B. In both cases the methods where evaluated under white (a, c) and 1/*f* (b and d) noise conditions for three OTCs. The output SNR of the GQSD for $M = 1$ is not estimated since the reconstruction of the gated signal is non-periodic. On the other hand, a gate of 1sample is used by the SMGI to detect the peak voltage of the input pulse.

V. Results and Discussion

A. Simulation Results

The SNR performance of GQSD and SMGI was recorded for Case A, B and C under various input conditions. The output SNR values for each method are plotted in Fig 10 and Fig 11, as bar charts where the black and grey bar series correspond to the performance of GQSD and SMGI respectively. The results of Case A are shown in Fig. 10a for white noise and Fig. 10b for 1/*f* noise. Similarly, Fig. 10c and Fig. 10d depict the performance of the two methods for Case B. Results for Case C are presented in Fig.11. The results are consistent for varying gate size, varying OTC, as well as type of pulse. The variations depending on the type of noise are presented and discussed below.

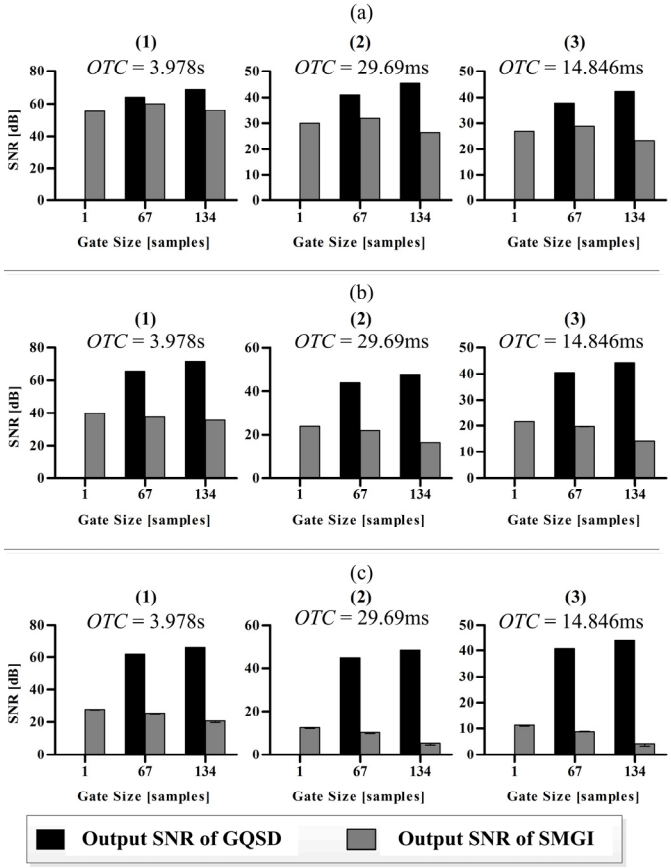

Fig. 11 SNR performance of GQSD and SMGI to an arbitrary shaped pulse train signal with accompanied noise proportional to $1/f^{(\beta)}$. The value of the exponent β was set to 1.58, 2.04, and 2.51 for (a), (b), and (c) respectively. Similarly to Case B, the output SNR of the GQSD for $M = 1$ is not estimated, since the reconstruction of the gated signal is non-periodic.

1) White Noise

The results in Fig. 10a and Fig. 10c imply that for white noise the SNR performance of SMGI is superior to GQSD for the lower two gate sizes. In the example case shown in Fig. 10a.2. even though for a gate size of 136 samples the SNR output of GQSD (49.5dB) is higher than SMGI (46.2dB), this is not sustained for a smaller number of samples. The SNR performance of SMGI increases to 52.5dB when the gate size is decreased to 62 samples.

The reduction of the gate size caused the output signal of SMGI to increase from 18.054mV to 44.961mV and the output noise from 88.45μV to 106.74μV. In comparison, the GQSD output increases from 15.85mV to 15.94mV whereas the noise from 53.86μV to 82.48μV. In both methods, the output noise was observed to be higher since the f_{eff} was increased to maintain the same OTC. Even with lower output noise, the SNR of GQSD is overall less than the SMGI under Gaussian white noise conditions. These are expected results, since the SMGI measures the peak amplitude of the pulse which is substantially higher than the magnitude of the fundamental harmonic of the gated signal $s_G(k)$ used in GQSD.

2) 1/f noise

The SNR performance of GQSD improves in the case of *1/f* noise as shown in Fig. 10b and Fig. 10d. This is exemplified in charts (2) and (3) where the performance of the two methods becomes comparable already for the intermediate gate sizes. A significant improvement in GQSD against SMGI is notable for higher bandwidths where the OTCs values are reduced to achieve higher detection rates. At slower rates, the SNR of SMGI improves due to a substantial decrease of the output noise while the output signal level is maintained at a voltage much higher than the GQSD.

The results obtained in Case C are shown in Fig. 11 where the two methods were tested under various types of colored noise proportional to $1/f^{\beta}$ by varying the exponent factor β. For consistency with previous simulations, the evaluation settings and pulse type are identical to Case B. The bar charts in Fig. 11a, Fig. 11b, and Fig. 11c represent the SNR performance of the two methods for $\beta = 1.5$, $\beta = 2$, and $\beta = 2.5$ respectively. As speculated, the performance of SMGI exacerbates as β increases while the SNR response of GQSD remains unaffected. The increase of β results to a steeper slope of the PSD noise curve as shown in Fig. 7. Naturally, the low frequency components of $1/f^{\beta}$ noise are dominating critically the baseband region causing the SMGI output noise to increase. On the other hand, the GQSD operates at 2kHz where the $1/f^{\beta}$ noise is much less, hence the SNR advantage. As discussed in Section II, this is a consequence of the input signal being modulated at a higher frequency with subsequent QSD.

B. Performance Comparison on Acquired and Simulated Data

To partially validate our evaluation procedure for comparing the two methods, and particularly the deployment of our noise models, GQSD and SMGI were applied separately and in real time on two types of data trains: acquired from an experiment, as well as simulated as described in IV. The time domain signals shown in Fig. 12a and b represent the acquisition and simulation, respectively, of the detected pulsed modulated signal. The simulated signal used for comparison was obtained by feeding an ideal pulse train to a LabVIEW model of a trans-impedance amplifier mimicking the conversion of the pulsed photodiode current to a voltage signal. The timing properties of the ideal pulse train are set equal to the real time signal that drives the laser source. Subsequently, the gain and time constants of the Labview trans-impedance amplifier were appropriately configured to match the output of the acquired real-time photodiode signal.

To recreate the noise contribution in the acquired signal, the voltage response of the PIN photodiode was recorded under no irradiation (dark) conditions. The FFT of the detected signal was then passed through an RMS averaging algorithm to reduce the fluctuations of the constituent noise harmonics without reducing the actual noise floor. Fig. 12c shows the approximation of the noise floor achieved after taking 1000 averages. The spectrum of the input noise is proportional to $1/f^{\beta}$ where Δx and Δy are extracted from the graph and substituted in (18) yielding $\beta \approx 1.7$, which was then passed to the noise

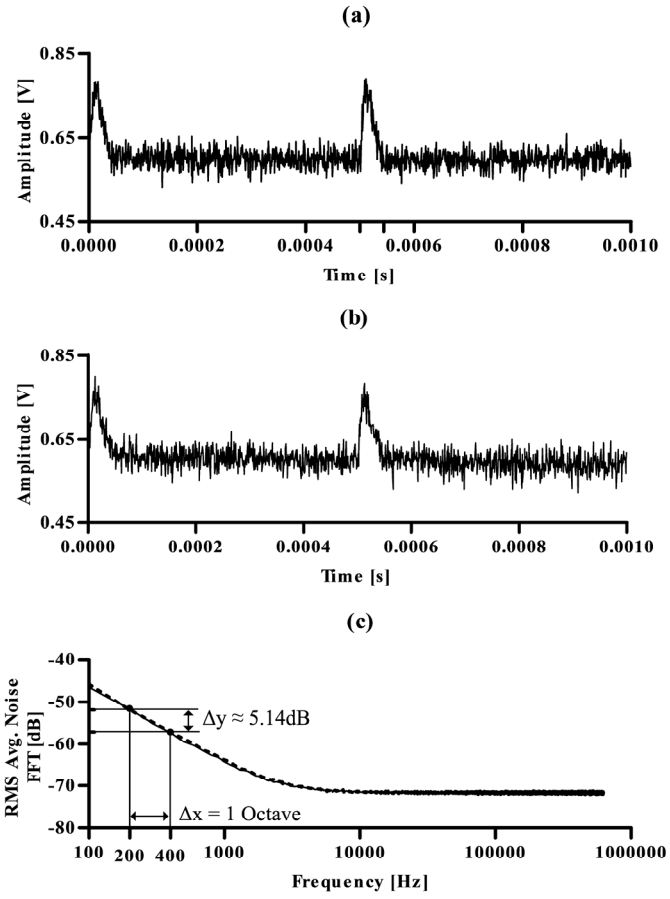

Fig. 11 Acquisition (a) and simulation (b) of temporal voltage response of PIN Photodiode to a pulsed laser diode emission. The FFT of both signals is shown in (c) where linear RMS averaging is performed to estimate the exponent β as the slope of the noise curve.

generation subroutine to simulate accurately the experimental noise conditions. In Fig. 12c. the error between the simulated (dotted line) and real time (solid line) noise spectra is negligible, making the two plots indistinguishable.

The overall comparison between the SNR performance of GQSD and SMGI, on acquired and simulated data, is shown in Fig. 13a and Fig. 13b respectively. The excellent match of the results justifies the use of the SPS to investigate the performance of GQSD and SMGI under various types of pulsed signals. Secondly, the obtained results are in line with those obtained for Case C on simulated data only, where we concluded that for $\beta \geq 1$ the performance of SMGI becomes poor as opposed to GQSD. Indeed, for $\beta \approx 1.7$ the SNR obtained by GQSD is improved by approximately 15 dB. It is interesting to comment here on the possible real-time performance of systems implementing GQSD. In the simplest and least demanding case of low repetition rate, stationary pulse trains, an initial calibration and setup phase is required to establish the optimal GW for a certain shape of the detector response; that is adequate to manage the real time acquisition and processing. In the other end of complexity is the case of high repetition rate, dynamic pulse trains. Here the calibration and setup provides only the starting optimal GW value.

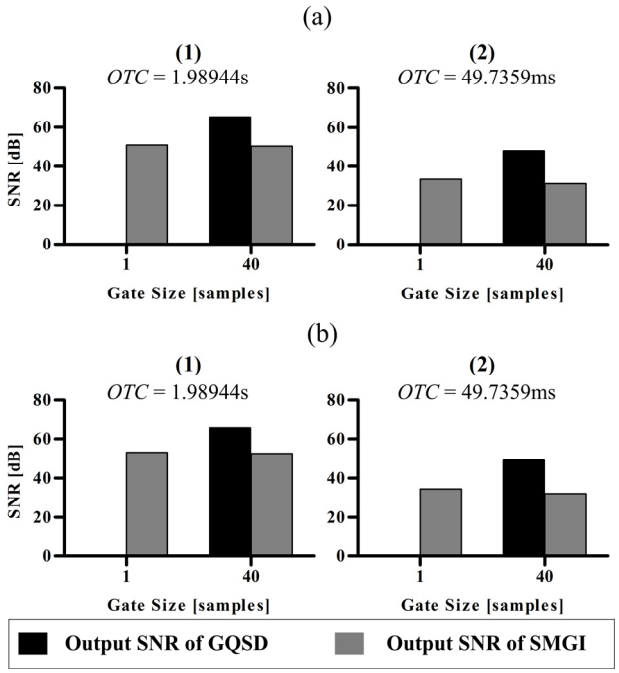

Fig. 13 SNR performance of GQSD and SMGI in a real-time experimental setup. Experimental SNR results are shown in (a.1) and (a.2) corresponding to an OTC of 1.989s and 49.7359ms respectively. Similarly the SNR performance of the simulated input signal is shown in (b.1) and (b.2).

The latter may change in real time if the shape of the response changes across the dynamic range of the detector. Therefore analyses and correction needs to be applied in real time to avoid unacceptable errors in recovering $\mathfrak{I}_{G1}$. The suitability of any algorithm for this will depend heavily on the character of every particular case, and in general will consume more resources, e.g field programmable logic and/or other hardware acceleration

At this point, it is worth mentioning that the improved SNR performance does not result in compromising the real time character of the signal processing. The gating block of GQSD captures the desired part of the period for each acquired pulse, and feeds in real time the improved duty cycle signal to the QSD block. Obviously, the gating process results in a "dead time" interval, which does not contribute to the final signal. Thus, because of the elimination of unneeded samples, the input to the QSD block appears modulated at a higher frequency than the initial signal period. This requires a certain delay in the processing, which is accounted for in the calculation of the OTC, but this delay does not affect the real-time performance. Furthermore, the delay does not involve a filtering process, which implies that GQSD achieves its improved performance with less demanding filtering and effectively shorter time constants compared to CQSD or SMGI. Therefore, the implementation of GQSD, e.g. on microprocessor or FPGA targets, will result, in less intensive processing since the irrelevant parts of the input pulse train will be discarded.

In summary, the key motivation and goal in this work is to establish a new method for pulse signal detection and establish the performance envelope in which it outperforms the existing ones. For low duty cycle pulse trains, the sensitivity and efficiency of CQSD is greatly reduced because of the increased energy spread across the spectrum, leading to deterioration in the SNR. SMGI is the method of choice for pulsed signals, but does not offer immunity against $1/f$ noise and, when the latter is overwhelming, CQSD becomes the better choice. Combining the principles of "gating" and "synchronous demodulation" we propose a new signal processing method, Gated Quadrature Synchronous Detection (acronym GQSD), which is efficient against $1/f$ noise and in improving the output SNR. It incorporates a gating function to achieve signal conditioning suitable for synchronous detection, while the baseband shifting followed by QSD ensures minimum effect of Flicker noise. A possible advantage of applying GQSD with low bandwidth devices, such as a PED, will be that it allows a nominally slow detector to be exploited at higher than usual frequencies. This is possible, since gained reserve in SNR can be traded against sensitivity, e.g. by reducing the electrical time constant.

REFERENCES

[1] P. H. Sydenham, "Handbook of Measuring System Design," T. Richard, Ed., 1st ed: Wiley, 2005, pp. 1227-1228.
[2] R. Shenoy, J. Ramakrishna, and K. Jeffrey, "A simple and inexpensive two channel boxcar integrator," *Pramana,* vol. 13, pp. 1-7, 1979.
[3] S. G. Castillo and K. B. Ozanyan, "Field-programmable data acquisition and processing channel for optical tomography systems," *Review of Scientific Instruments,* vol. 76, pp. 095109-6, 2005.
[4] S. G. Castillo and K. B. Ozanyan, "Generic-type hierarchical multi digital signal processor system for hard-field tomography," *Review of Scientific Instruments,* vol. 78, pp. 055102-9, 2007.
[5] J. M. Masciotti, J. M. Lasker, and A. H. Hielscher, "Digital Lock-In Detection for Discriminating Multiple Modulation Frequencies With High Accuracy and Computational Efficiency," *IEEE Transactions on Instrumentation and Measurement, ,* vol. 57, pp. 182-189, 2008.
[6] J. L. Collier, B. J. Goddard, D. C. Goode, S. Marka, and H. H. Telle, "A low-cost gated integrator boxcar averager," *Measurement Science and Technology,* vol. 7, p. 1204, 1996.
[7] J. Gal, "Double gated-integrator for shaping nuclear radiation detector signals," *Nuclear Instruments and Methods in Physics Research Section A: Accelerators, Spectrometers, Detectors and Associated Equipment,* vol. 462, pp. 506-518, 2001.
[8] N. P. Reddy and N. B. P. Reddy, "Digital double boxcar integrator for pulsed NMR experiments," *Electronic Circuits and Systems, IEE Proceedings G,* vol. 129, pp. 245-249, 1982.
[9] J. Reichert and J. Townsend, "Gated Integrator for Repetitive Signals," *Review of Scientific Instruments,* vol. 35, pp. 1692-1697, 1964.
[10] D. W. Swain, "Boxcar Integrator Attachment for Oscilloscopes," *Review of Scientific Instruments,* vol. 41, pp. 545-547, 1970.
[11] P. Williams and H. W. Lam, "Simple boxcar integrator covering a large input frequency range," *Journal of Physics E: Scientific Instruments,* vol. 18, p. 23, 1985.
[12] R. Suzuki, K. Umezu, H. Takuma, and F. Shimizu, "Multiple sampling digital boxcar integrator, an efficient signal averager," *Review of Scientific Instruments,* vol. 52, pp. 287-292, 1981.
[13] R. Hafiz and K. B. Ozanyan, "Optical Absorption Measurements in Particle-Containing Ambients Using Gated Ratiometric Detection," *Sensors Journal, IEEE,* vol. 8, pp. 1437-1444, 2008.
[14] S. Efthymiou and K. B. Ozanyan, "Pulsed performance of pyroelectric detectors," *Journal of Physics: Conference Series,* vol. 178, p. 012044, 2009.
[15] M. L. Meade, "Advances in lock-in amplifiers," *Journal of Physics E: Scientific Instruments,* vol. 15, pp. 395-403, 1982.
[16] H. Umer and A. Muhammad Sabieh, "Reducing noise by repetition: introduction to signal averaging," *European Journal of Physics,* vol. 31, p. 453, 2010.
[17] S. Efthymiou and K. B. Ozanyan, "Advanced simulator of pyroelectric detector circuits and associated signal processing," in *AFRICON, 2011*, pp. 1-6, 2011.
[18] B. P. Lathi, *Signal Processing and Linear Systems*. India: Oxford University Press, 2000.
[19] S. Efthymiou and K. B. Ozanyan, "Sensing of pulsed radiation with Pyroelectric Detectors," in Proc. *SENSORS, 2010 IEEE*, pp. 1372-1376, 2010.

[20] N. R. Moloney, K. Ozogány, and Z. Rácz "Order statistics of $1/f^{\alpha}$ signals", *Physical Review E*, Vol. 84, p.061101, 2011,

Spyros Efthymiou received his BSc and MSc degree in Electrical (2007) and Electronic Engineering and Sensors and Electronic Instrumentation in 2008 respectively, from the University of Manchester, Uk. After receiving a PhD degree focused on sensors and digital signal processing, he is currently employed by ABILITY (Switzerland, Zürich) as an R&D engineer.
His current interests are in the area of electronic circuit design (digital or analogue), digital signal processing and signal recovery. He is currently responsible for the research department of ABILITY involving robotic rehabilitation devices for stroke and spinal cord injured patients.

Krikor B. Ozanyan (M'1995, SM'2003) received his MSc degree in engineering physics (semiconductors) and PhD degree in solid-state physics, in 1980 and 1989 respectively, from the University of Sofia, Bulgaria.
He has held previous academic and research posts in the University of Sofia, The Norwegian Institute of Technology (Trondheim, Norway), the University of Hull (UK), and the University of Sheffield (UK), working on projects ranging from Brewster-angle mid-IR spectroscopic ellipsometry and electron confinement in quantum wells and barriers, to the demonstration of the lasing at 333nm from strained MQW ZnCdS/ZnS structures and *in-situ* real-time optical monitoring of growth of III-V semiconductors in MBE and MOCVD reactors. His current interests are in the area of photonic sensors and indirect imaging (tomography) by optical modalities, signal processing for optical experiments, and spectroscopy with ultrafast laser sources. He is currently Head of Sensors, Imaging and Signal Processing at the University of Manchester and Adjunct Professor at the University of Bergen, Norway.
Professor Ozanyan is Fellow of the Institute of Engineering and Technology, (UK, formerly IEE) and Fellow of the Institute of Physics (UK). He was Distinguished Lecturer of the IEEE Sensors Council in 2009-2010, Guest Editor of the IEEE Sensors Journal Special Issues "Sensors for Industrial Process Tomography" in 2005 and "THz Sensing: Materials, Devices and Systems" in 2012. He is currently Editor-in-Chief of the IEEE Sensors Journal.